

Adaptive Cost Coefficient Identification for Planning Optimal Operation in Mobile Robot based Internal Transportation

Pragna Das, Lluís Ribas-Xirgo, *Member, IEEE*

Abstract—Decisions in automated logistic systems can be improved based on knowledge of real-time state of individual parts and also environmental factors. These knowledge can be obtained through travel time of edges by individual robots which represents the utility based costs in the system. Our work focuses on identifying cost coefficients in an autonomous multi-robot system used for internal transportation. With suitable predictions of these travel times the current status of cost involved in traversing from one node to another can be known. Thus suitable state-space model is formulated and Kalman filtering is used to estimate these travel time to use as weights for cost efficient route planning. Experiments show that paths obtained using online travel times as weights have total traversing cost reduces by 15% on average.

Index Terms—Multi-robot systems, planning and co-ordination, cost parameter, parameter estimation, cost efficiency, Kalman filtering.

I. INTRODUCTION

MULTI-ROBOT systems (MRS) used for internal logistics in factories demand robust fault tolerant, adaptable and cost efficient planning and co-ordination. Cost efficient planning in MRS involves many problems where decisions are to be based on information obtained during functioning of the system [3], [8], [13]. Figure 1 illustrates a scaled

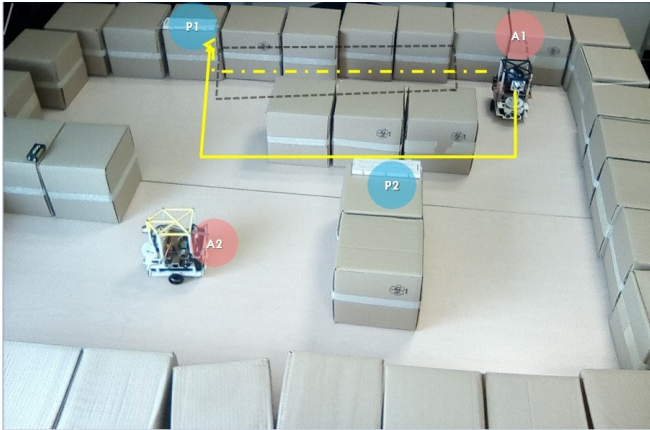


Fig. 1: An example

down automated internal transportation system, typically used for logistics in factories and executed by automated guided vehicles (AGVs) or mobile robots (MRs). In this example, all AGVs can execute only one task at a time. Let, at t_i , A1 have to carry some material to P1 and the path computed is marked by the dotted line. Again, at time t_j ($j > i$), A1 needs to carry same material to P1. But now, the battery capability of A1 has decreased due to execution of previous tasks and the condition of the given path has deteriorated (as marked by dotted rectangle). Hence, equal amount of time and energy as previous would not be sufficient to reach P1 at t_j .

In this case, dynamic planning and co-ordination can be improved based on various forms of utility [13] like capability, quality, fitness, reward, *et cetera*. These utilities can be directly related to time(s) needed to perform task(s) by individual robots [16] in the system and can influence not only the efficiency of each MR but also the whole system [13]. Hence, these quantities are formalised in order to incorporate the conditions of the different environmental, physical and mechanical factors of any MRS into the control decision steps as cost coefficients to exhibit a quantitative measurement of utility [13]. In Figure 1, the cost needed to traverse to P1 considering the floor condition must be estimated for A1. Then a different path can be computed considering these factors, for example the path marked by solid line can be a better decision to traverse to P1.

Aforementioned cost coefficients can be of individual robots in MRS, irrespective of the kind of task the robot needs to perform. On one hand, they arise locally at each individual AGV due to action of actuators, wheels and other mechanical factors. But they are significantly influenced by environmental factors like battery capacity (in case of battery powered MRs), conditions of the floor, conditions of material to be transported, performance and behavior of other AGVs, *et cetera*, as all or most of these factors determine the state of the robot at every instance of time. Influence of factors like friction forces of floor, slope, mechanical part can be corrected by local control on individual AGV (lower levels), but factors like traffic condition, conditions of material, behavior of other AGVs are beyond the scope of control by lower levels. Hence, considering cost coefficient at lower levels of actuation and control cannot make better control decisions. So these parameters are investigated at higher level to utilize them efficiently. These costs are time dependant and have sources of error from battery exhaustion, surface condition of shop floor, wear and tear of tyre, *et cetera*. Hence over the passage of

P Das is with Microelectronics and Systems Electronics Department, Autonomous University of Barcelona, Bellaterra, Barcelona, 08193 Spain e-mail: (pragna.das@uab.cat).

L. Xirgo is with Microelectronics and Systems Electronics Department, Autonomous University of Barcelona, Bellaterra, Barcelona, 08193 Spain e-mail: (lluís.ribas@uab.cat).

time, the values will change.

In case of the task of path traversal from one port to another, travelling time can be thought of one such cost factor which determine the utilities based not only on internal factors of each robot but also on environmental factors. The efficacy of the aforementioned cost coefficients is shown by calculating travelling cost between paths obtained by heuristically gathered cost and real travelling cost (as estimated using cost factor) irrespective of the route planning method.

Traditional path planning algorithms like Dijkstra's algorithm can be applied by modifying the cost of one edge from distance to estimated travelling time. This will help to produce paths with less cost.

Average path cost obtained using static estimation of travel time (variation of edge travel cost over time is not considered) shows an improvement over heuristically obtained path cost by roughly 5% on average (Section V).

In reality, edge costs or travelling times of edges vary along time and require to be predicted accordingly during path planning. A good estimation method to accurately predict travel times requires histories of edge costs, which can be collected progressively during MR operation. During the learning phase, the filtering method cannot generate the best estimates and least cost path cannot be produced. The estimates get improved over time. Real traversing costs are obtained by these estimations which can produced different paths than that of other costs like theoretical, heuristic and experimental. In fact, estimating traversal time by Kalman filtering shows that heuristic edge costs can underestimate total costs and, thus, can lead to non-minimal paths.

The contribution of this paper is twofold. Firstly, edge traveling time is identified as a suitable cost coefficient considering an analogy to real, automated and fully functional plant. Secondly, these identified travel times are estimated both statically and dynamically. Further to this, they are utilised in a planning control decision making process to culminate into better optimal results for each MR in order to obtain more cost efficient performances of MRs.

II. BACKGROUND

So far, path planning has been solved in two distinctly different approaches for autonomous robots. Sampling methods perform reasonably well in solving intricate path planning problems in static and dynamic environment for a single robot [11]. The vehicular dynamics are considered as state in these approaches and the minimum cost path is obtained by spanning the search tree based on the distance between the current state and goal state. Although Suh and Oh in [21] and Achtelik *et. al* in [1] have used Gaussian process as the cost of the path to incorporate environmental parameters, the search mandates to conceive the vehicular dynamics of the robot. Also, sampling based methods are blocked into local minima and uncertainties in the environment hinder successful results [11]. Further, heuristic approaches like Artificial Neural Network (ANN) [9], Genetic Algorithm (GA) [2], Particle Swarm optimisation (PSO) [22], Ant Colony Optimisation (ACO) [6], *et cetera* can adapt to uncertainties and changing

environment. But, they are computationally expensive which is a major concern for robotic control units equipped with limited resources and real-time constraints [14]. The vehicular mechanical factors and environmental factors are incorporated in travel times in this work to mitigate the identification of the vehicular dynamics. The path is computed in higher level of robotic control and paths are broken down to simple vehicular commands for movements and communicated to the lower-levels of control. Also, simple, deterministic and computationally inexpensive Dijkstra's algorithm is deployed and travel times are incorporated with it to decide paths of minimum cost.

On the other hand, motion planning and task planning, serves as specific coordination problems in MRS. Cost coefficients are usually computed heuristically before hand (offline) using Markov Decision Processes (MDPs). However, motion planning and task planning, as a specific case of coordination problem, are typically NP-hard and are addressed to find tractable and good solutions [10] and are mostly treated as individual specific problems in field of MRS [5], [12], [20].

In this work, path planning has been considered as an example of planning, where travel times are utilized as costs to obtain optimal path in a single robot.

III. PROBLEM FORMULATION

In this work, the focus is on one AGV. A path P for a robot is usually defined as,

$$P = \langle (n_a, n_b), (n_b, n_c), (n_c, n_d), (n_d, n_e), \dots \rangle \quad (1)$$

In this work, traversing a path is considered as a task (Section I). As explained in Section I, each edge in the floor map is associated with some cost in terms of energy exhaustion and others. Hence, traversing a defined path incurs several travel costs for all edges in the path. Thus time to traverse an edge by a MR can be conceptualized as its cost coefficients. Let $X_{p,q}(e, f)$ denote edge cost from n_p to n_q , where e denotes dependency for state of charge of batteries and f denotes dependency for frictional force of the floor. Now, the cost of traversing P can be written in a form P_c as,

$$P_c = \langle (X_{a,b}(e, f), X_{b,c}(e, f), X_{c,d}(e, f), \dots) \rangle \quad (2)$$

From now, $X_{p,q}(e, f)$ will be written as $X_{p,q}$ for simplicity. For continuous performance of the MR, path computation needs to be repeated once a destination is reached. Thus, P_c for every call to path planning can be expressed as,

$$P_c^i = \langle (X_{a,b}^i, \dots, X_{d,e}^i, X_{e,g}^i, \dots, X_{q,r}^i) \rangle \quad (3)$$

where i denotes the number of computation of path. A MR may need to traverse the same edge in different calls of path planning (Section I). Now, for j th call for path planning when $j > i$, let P_c be,

$$P_c^j = \langle (X_{d,e}^j, X_{e,g}^j, \dots, X_{q,r}^j, \dots, X_{w,x}^j) \rangle \quad (4)$$

In equation 3 and 4, there are common edges for example, from n_d to n_e , n_e to n_g , *et cetera*. Thus, it is observable in equations 3 and 4 that P_c^i and P_c^j can have many common $X_{p,q}$ elements, though the values will not be the same. The reason being the discharge of batteries and (or not) possible change of environment. Thus, travel time from n_p to n_q ($X_{p,q}$)

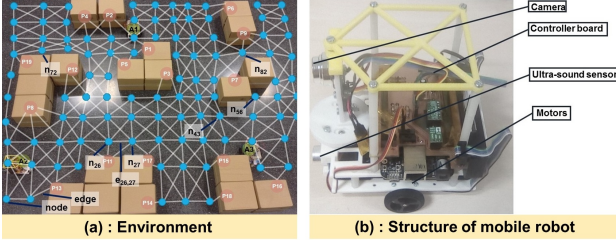


Fig. 2: Scale down prototype platform

becomes a function of k as $X_{p,q}(k)$ where, k = number of time a MR traverses any edge. Thus the dependency of travel time $X_{p,q}$ over state of charge of batteries and frictional forces are captured through its variation with the increase of traversed edges. The elements of P_c are identified for each call of path planning. For example, $X_{d,e}$ is needed to be estimated for a different k value in P_c^j than P_c^i . Hence, $X_{p,q}(k)$ is estimated with respect to increase in k for any edge and used as weight of edge to compute path. The estimated value of $X_{p,q}(k+1)$ depends only on $X_{p,q}(k)$ and the observation of $X_{p,q}$ at $(k+1)$. These experiments and results are explained in Section V. Observations of all possible $X_{p,q}(k)$ for all possible k needs to be made for this above estimation for a single AGV.

However, this is not only cumbersome but also impractical to gather such huge amount of observation. This estimation is static as X is estimated without considering its variation with the total elapse of time from start of system. The static estimation approach is progressed to a different model. In this approach, observations of all possible $X_{p,q}(k)$ for all possible k is not needed. The model is allowed to gather the possible values of $X_{p,q}$ itself from the beginning of first call of path planning and use these values to estimate current value. A window of previous values of $X_{p,q}$ is decided. The estimated value of $X_{p,q}(k+1)$ depends on this window or set of previous $X_{p,q}(k)$ s along with the variation of exploration of $X_{p,q}$ due to elapse of time. Thus, X values are dynamically estimated considering its variation over elapse of time.

IV. PROTOTYPED INTERNAL TRANSPORTATION SYSTEM

A prototype scaled down internal transportation system is developed with all essential constituting parts like MRs, tasks, controller architecture and the environment adhering to minute details. The floor is described by means of a directed graph $\mathcal{G} = \{\mathcal{V}, \mathcal{E}\}$, where each port and bifurcation point corresponds to some node $n_r \in \mathcal{V}$ and each link between two nodes forms an edge $a_{e,f} \in \mathcal{E}$. Part (a) of Figure 2 depicts a portion of the whole prototype, where, notation like n_{26} designates a node and $a_{26,27}$ a edge. Topological graphs are generated based on a simple assumption, that each free cell in the grid map corresponds to a node in the graph, taking reference from the grid map generated by results of Self Localisation and Mapping (SLAM) in [4] from the automated factory of Coca-Cola Iberian Partners in Bilbao, Spain. A selected representative portion from each of the three sections of of Coca-Cola Iberian Partners in Bilbao, Spain are extracted to form three topological maps. They are provided in Figure 3. Part (a) of Figure 3 illustrates Map 1 which is a representative of winding racks in the warehouse facility,

Part (b) shows Map 2 which represents randomly placed racks and Part (c) shows Map 3 which represents racks organized in a hub. The scaled robots are built controller, ultrasound sensor and a camera, as illustrated in Part (b) of Figure 2. The DC servo motors drive the wheels of the MR and Li-ion batteries energize them. Each MR has its individual controller in decentralized architecture [18], [19].

Travel times for three different length of arcs in all three maps and four different conditions of surface are recorded till complete exhaustion of batteries. This generates observation data for all possible $X_{p,q}$ for all k s. For example, (b) plots the progressive mean of observed values of $X_{68,69}$, where $a_{68,69}$ be m th edge in Map1 inside the zone marked in Figure 4, first only with the change of state of charge of batteries (left plot) and second with both the change of state of the charge of batteries and the floor condition from rough at the beginning to smooth (right plot). Part (a) of Figure 5 plots the cell voltage over time of Li-ion batteries.

The cell voltage in (a) decreases for the first, then resorts to a steady value for a long time and then decreases steadily till full discharge. The plot of progressive mean of $X_{68,69}$ in left plot of (b) shows that the values increase first, then steadily decrease and then increase gradually till complete discharge. But the longer increase of values of $X_{68,69}$ in right plot can be attributed to the rough floor, because at equal battery capacity in both cases, more energy is required to traverse in rough surface. Plot of $X_{p,q}$ the same arc in different conditions of floor demonstrate that $X_{p,q}$ can reflect not only state of charge of batteries [?] but also environmental conditions. The above huge and cumbersome process of acquiring the observations for generating on-line estimates is mitigated by a non-linear functional model of $X_{p,q}$ incorporating its evolution over passage of time and also allowing to gather information about $X_{p,q}$ for different arcs in the map gradually with time.

V. EXPERIMENT I: OBTAINING OPTIMAL PATH USING ESTIMATES OF STATIC COST

A. Procedure

The state-space model provided in equations 5 and 6 is used to estimate edge travel cost. From now $X_{p,q}$ will be written as X for simplicity,

$$X(k) = X(k-1) + \omega(k) \quad (5)$$

$$Y(k) = X(k) + \eta(k) \quad (6)$$

The state vector in equation 5 is a single variable X depending on k , k being the number of edges already found in the path (Section III). Hence, X is estimated over and over again for different connecting edges of every new exploring node. $Y(k)$ in equation 6 is the observation variable for X . This model involves two error terms $\omega(k)$ and $\eta(k)$ which are independent and normally distributed. According to equations 5 and 6, $X(k)$ depends only on the travel time of edge between current node and its predecessor i.e.- $X(k-1)$. Equations 7 and 8 are obtained after applying Kalman Filtering method [put reference] on equations 5 and 6.

$$\begin{aligned} \hat{X}^-(k) &= \hat{X}(k-1) \\ P^-(k) &= P(k-1) + \sigma_\omega^2 \end{aligned} \quad (7)$$

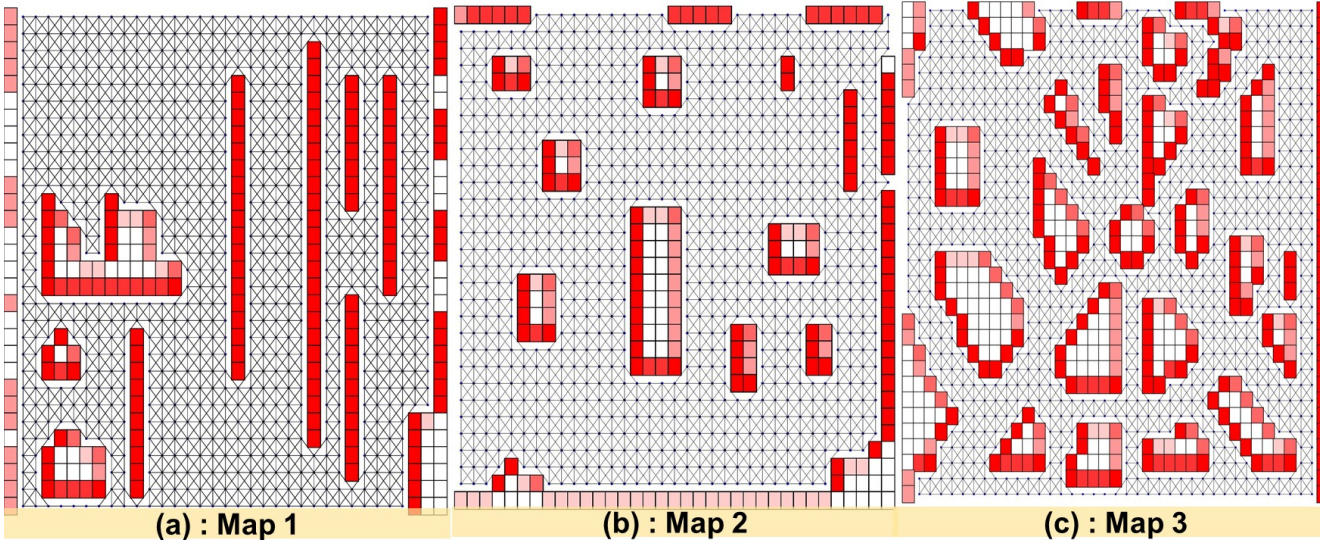


Fig. 3: Three representative topological maps

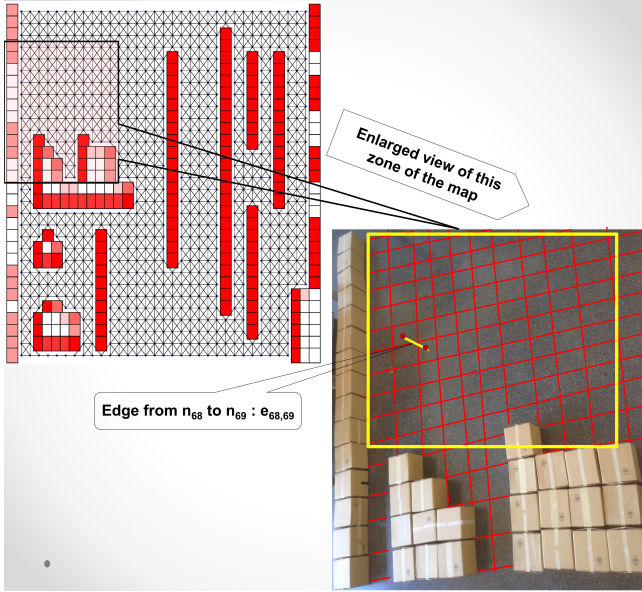


Fig. 4: Surface condition

$$\begin{aligned}
 K(k) &= P^-(k) / [P^-(k) + \sigma_\eta^2] \\
 P(k) &= P^-(k) - [P^-(k)^2 / [P^-(k) + \sigma_\eta^2]] \\
 \hat{X}(k) &= \hat{X}^-(k) + [P^-(k) / P^-(k) + \sigma_\eta^2] * \omega(k) \quad (8) \\
 \text{where, } \omega(k) &= [Y(k) - \hat{X}^-(k)]
 \end{aligned}$$

$\hat{X}^-(k)$ produces the apriori value of X and P^- produces the associated covariance, σ_ω^2 being the covariance of process noise $\omega(k)$. $\hat{X}(k)$ provides the predicted estimate of $X(k)$, as $\hat{X}^-(k)$ is corrected in equation 8 with the help of Kalman Gain $K(k)$. $P^-(k)$ provides the associated covariance matrix, σ_η^2 being the covariance of the observation noise $\eta(k)$. For example, a sample route computation is illustrated in Figure 6. Let n_a be source and n_{56} destination at P16. So, path computation using Dijkstra's algorithm starts at n_a with its neighbors n_b , n_c and n_d . So, $X_{a,b}$, $X_{a,c}$, $X_{a,d}$ are required to be estimated at k . At the beginning, there is no previous

edges traversed. So, value of k will be 1 at the start.

$$\hat{X}(0) = E[X(0)] \quad (9)$$

$$P(0) = E[(X(0) - E[X(0)])(X(0) - E[X(0)]^T) \quad (10)$$

We use equation 7 to obtain $\hat{X}^-(1)$ for $X_{a,b}$, $X_{a,c}$, $X_{a,d}$ separately depending on $X(0)$ using equation 9. Similarly, we get separate $P^-(1)$ using equation 10. Next, we obtain $\hat{X}(1)$ (estimate) and $P(1)$ for $X_{a,b}$, $X_{a,c}$, $X_{a,d}$ using equation 8. Comparison of estimated values of $X_{a,b}$, $X_{a,c}$, $X_{a,d}$ will provide the least cost edge from n_a . Let, the least cost edge be $a_{a,c}$. So n_a will become the predecessor of n_c , i.e.-to reach n_c , the edge should come from n_a . When n_c will be explored, the value for k is 2 as n_c has 1 predecessor. The next least cost edge from n_c in the path is required to be known. Thus, $X_{c,e}$, $X_{c,f}$, $X_{c,g}$ needs to be estimated. Thus, observation $Y(k)$ of X at current k is required to estimate X . Thus observation values for travel costs of all possible X s for all possible k s were collected. This above process is explained in Algorithm 1.

Though, $X(k)$ varies only on $X(k-1)$ in this model, in reality, it depends on X s for all the previous edges in the path and its own variation over the time. Thus, this process of estimation is static (Section III). This static experiment is conducted to verify that weights of edges can be estimated online during exploration of Dijkstra's algorithm using a state-space model. Also, it is verified that the estimated values of X are correct and real through this experiment, as the values can be compared to real observations.

B. Results

Paths are computed repeatedly for 20, 40, 60 and 80 times in each topological graph (Figure 3) using both original Dijkstra's algorithm using Euclidean distance based heuristic weights of edges and the modified one (Algorithm 1). The choices of source and destination are fed from the decided list of sources and destinations for each call of route computation. Total path costs obtained using heuristic weights are compared with paths obtained using Algorithm 1. The vertical bars of *Eucl* and *SEC* in Figure 7 represent the average total path costs for

Algorithm 1 Dijkstra's algorithm using estimation of travel time

```

1: function INITIALISE_SINGLE_SOURCE( $V, s$ )  $\triangleright$  Where  $V$ 
   - list of nodes,  $s$  - source, returns  $d[v]$  - attribute for each
   node,  $\pi[v]$  - predecessor for each node
2:   for each  $x_i \in V$  do
3:      $\pi[x_i] = \text{infinity}$ 
4:      $d[x_i] = \text{NIL}$ 
5:   end for
6: end function
7: function FIND_PREV( $(u, s)$ )  $\triangleright$  input:
    $u$ -current node,  $s$ -source node, returns:  $prevV$ -predecessor
   of  $u$ ,  $noPred$  - number of predecessors till  $s$ 
8:    $prevV = \text{compute predecessor of } u$ 
9:    $noPred = \text{count of predecessors till } s$ 
10: end function
11: function KF( $(pW, k, Y(k))$ )  $\triangleright$  input:
    $pW$ -value of travel time at  $k-1$ ,  $k$ -instance for estimation,
    $Y$ - observation variable, Returns:  $\hat{X}(k)$ -travel cost from  $u$ 
   to  $v$ 
12:   Apply KF on state-space model to obtain  $\hat{X}(k)$ 
13: end function
14: function FIND_COST( $u, v, k, pW, Y(k)$ )  $\triangleright$  Input:  $u$ -current
   node,  $v$ - neighbor node,  $k$ - instance of estimation,  $pW$  -
   cost between  $prevu$  and  $u$ ,  $Y(k)$  - observation of travel
   time between  $u$  and  $v$ , Returns:  $w$ - estimated travel_time
   (cost) from  $u$  to  $v$ 
15:    $w = \text{KF}(pW, k, Y(k))$ 
16: end function
17: function RELAX( $u, v, w$ )  $\triangleright$  Inputs:  $u$ -current
   node,  $v$ - neighbor node,  $w$ - estimated travel_time (cost)
   from  $u$  to  $v$ , Returns:  $d[v]$ -attribute for each node,
    $\pi[v]$ -predecessor of each node
18:   if  $d[v] > d[u] + w(u, v)$  then
19:      $d[v] = d[u] + w(u, v)$ 
20:      $\pi[v] = u$ 
21:   end if
22: end function
23: function MAIN( $V, \varepsilon, Y, s$ )  $\triangleright$  Inputs:  $V$ -list of nodes,  $\varepsilon$ -list
   of edges,  $s$ -source node,  $Y$ -observation matrix, Returns:
    $\pi[v]$ -predecessor of each node,  $w$ -edge weight matrix
24:    $P := \text{NIL}$ 
25:    $Q := \text{queue}(V)$ 
26:    $k := 0$ 
27:    $p\varepsilon[s] = 0$ 
28:    $w[p\varepsilon[s], s] = 0$  initialise_single_source( $V, \varepsilon, s$ )
29:   while  $Q! = \emptyset$  do  $u := \text{Extract min-priority queue}(Q)$ 
    $pV[u], npred = \text{find\_prev}(u, s)$   $k = npred + 1$   $pW =$ 
    $w[p\varepsilon[u], u]$   $P := P \cup u$ 
30:     for each  $v \in \text{Adj}[u]$  do
31:        $w[u, v] = \text{find\_cost}(u, v, k, pW, Y(k))$ 
32:       relax( $u, v, w$ )
33:     end for
34:   end while
35: end function

```

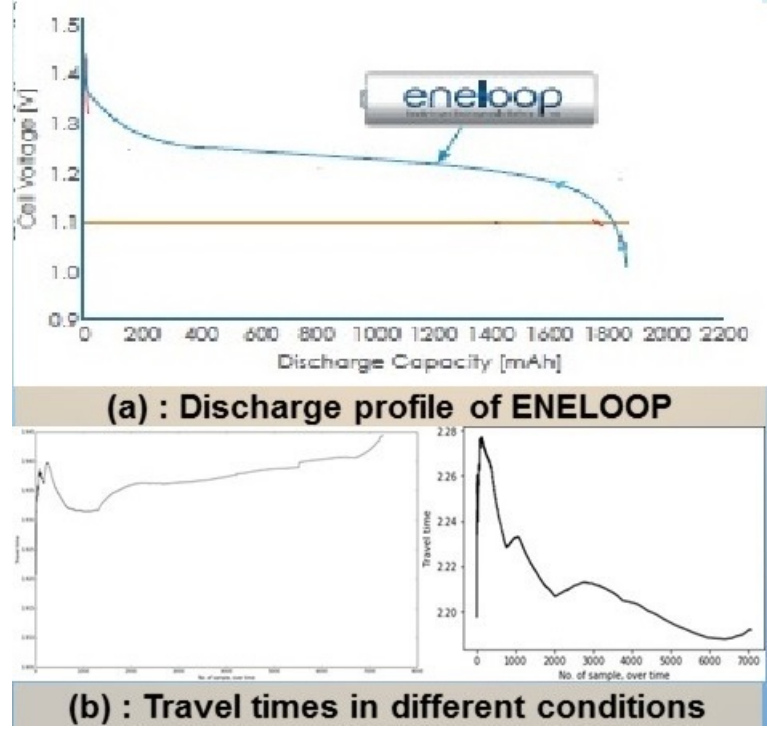


Fig. 5: Comparison between battery charge and travel cost

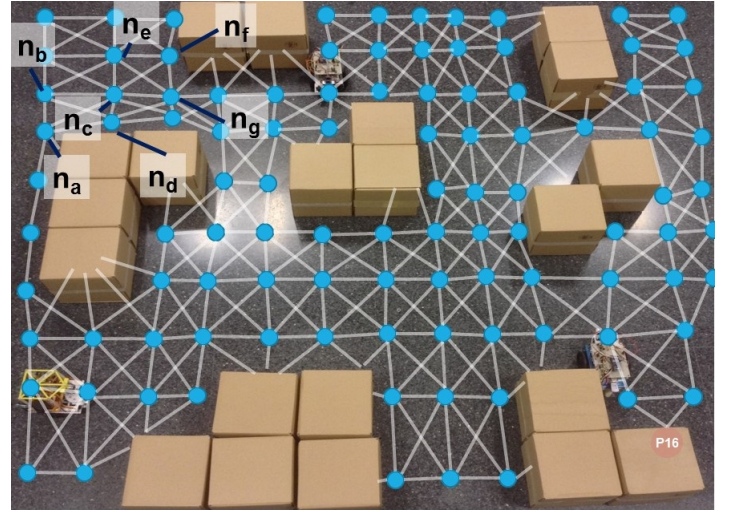


Fig. 6: Sample run of route computation

heuristic cost based routes and static estimates based routes respectively. Vertical bar *Eucl* shows that average total path costs never change with increase in number of repetitive calls, as heuristic weights do not change over time and does not reflect the true cost of traversal.

Vertical bar *SEC* shows that average total path costs obtained by Algorithm 1 is 5% less in case of Map 2 and Map 3 and 2% less in Map 1 than that of heuristic cost based Dijkstra's algorithm. Average total path costs increases with number of repetitions as shown by vertical bar *SEC*, as duration of performance increases with increase of repetitions. This happens due to the dependency of current edge cost on previous edge cost (equations 5 and 6). But, this variation does not truly reflect the variation of travel time due to time-varying

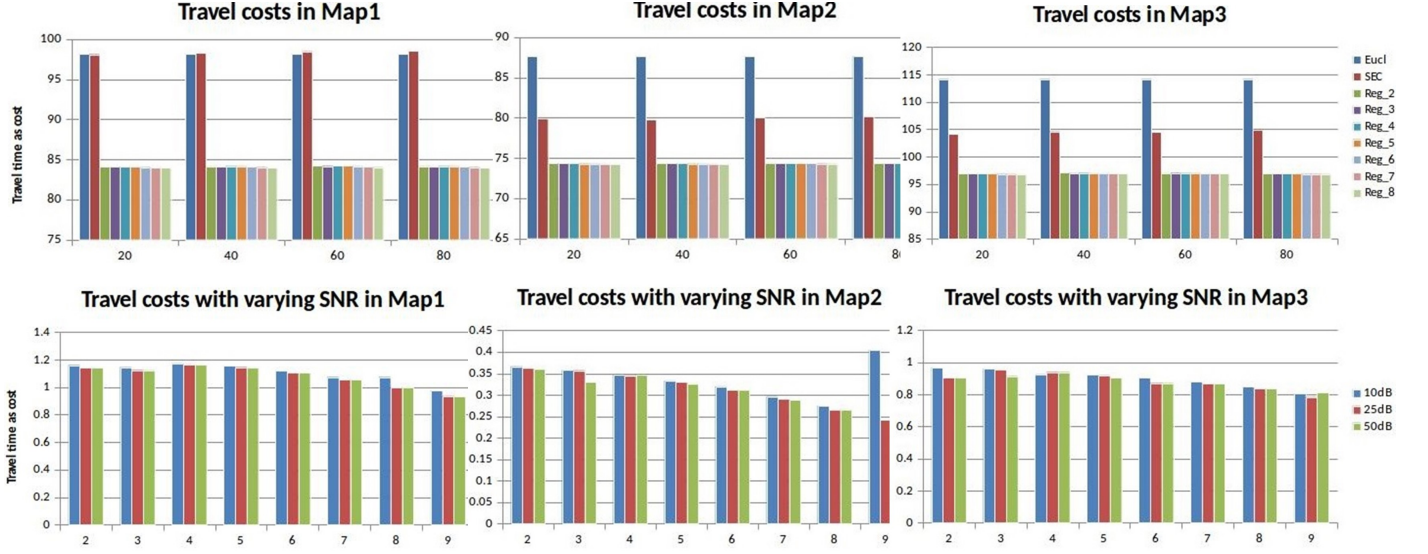


Fig. 7: Comparison cost

factors.

VI. EXPERIMENT II: OBTAINING OPTIMAL PATH USING ESTIMATES OF DYNAMIC COST

A. Procedure

The bi-linear model [17], provided in equation 11 is used to model the change of travel costs depending upon all the previous travel costs. X is formed as a function of its past histories over k , considering the progressive change ξ with respect to k . After start of computing a path, the real travel time of edges are recorded when the MR actually traverses it. This travel times of edges are used as the observation values for the next call of path planning. Thus observation values of travel times of each edge is grown during run-time.

$$\begin{aligned} X(k) + a_1 X(k-1) + \dots + a_j X(k-j) \\ = \xi_k + b_1 \xi(k-1) + \dots + b_l \xi(k-l) \\ + \sum \sum c_{rz} \xi(k-r) X(k-z) \end{aligned} \quad (11)$$

The double summation factor over X and ξ in equation 11 provides the nonlinear variation of X due to state of batteries and changes in environment. The state space form of the bi-linear model is given in equations 12 and 13. In equation 12, the state vector $s(k)$ is of the form $(1, \xi(k-l+1), \dots, \xi(k), X(k-j+1), \dots, X(k))^T$. Here, j and l denote number of previously estimated X s and previous innovations of X respectively. The term *regression_no* denotes the values of j and l and is chosen as a design parameter. The *regression_no* is increased from 2 to 9 and the effects on total edge travel cost of paths is demonstrated in Section VI-B.

$$s(k) = F(s(k-1))s(k-1) + V\xi(k) + G\omega(k-1) \quad (12)$$

$$Y(k) = Hs(k-1) + \xi(k) + \eta(k) \quad (13)$$

The state transition matrix F in the equation 12 has the form of

$$F = \begin{bmatrix} 1 & 0 & 0 & \dots & 0 & \vdots & 0 & 0 & \dots & 0 & 0 \\ 0 & 0 & 1 & \dots & 0 & \vdots & 0 & 0 & \dots & 0 & 0 \\ 0 & 0 & 0 & \dots & 1 & \vdots & 0 & 0 & \dots & 0 & 0 \\ 0 & 0 & 0 & \dots & 0 & \vdots & 0 & 0 & \dots & 0 & 0 \\ \vdots & \vdots & \vdots & \dots & \vdots & \vdots & \vdots & \vdots & \dots & \vdots & \vdots \\ 0 & 0 & 0 & \dots & 0 & \vdots & 0 & 1 & \dots & 0 & 0 \\ 0 & 0 & 0 & \dots & 0 & \vdots & 0 & 0 & 1 & \dots & 0 \\ 0 & 0 & 0 & \dots & 0 & \vdots & 0 & 0 & 0 & \dots & 1 \\ \mu & \psi_l & \psi_{l-1} & \dots & \psi_1 & \vdots & -\phi_j & -\phi_{j-1} & \dots & -\phi_1 \end{bmatrix}$$

The number of rows of F is given by $(2 * \text{regression_no} + 1)$. The ψ terms in F are denoted as in equation 14

$$\psi_l = b_l + \sum_{i=1}^l c_{li} X(k-i) \quad (14)$$

All the ϕ terms in F are constants. The term μ is the average value of X till k . Also, the matrix V in 12 is denoted as

$$V = \begin{bmatrix} 0 & 0 & 0 & \dots & 1 & \vdots & 0 & 0 & \dots & 1 \end{bmatrix}$$

The number of rows of V is again given by $(2 * \text{regression_no} + 1)$. The matrix H in 13 is denoted as

$$H = \begin{bmatrix} 0 & 0 & 0 & \dots & 0 & \vdots & 0 & 0 & \dots & 1 \end{bmatrix}$$

Kalman filtering is applied on the state-space model (equations 12 and 13) resulting in equations 15 and 17 to estimate s repeatedly to obtain X for the connecting edges at each node to compute path using Dijkstra's algorithm.

$$\hat{s}^-(k) = F(s(k-1))s(k-1) + V\xi(k) + G\omega(k-1) \quad (15)$$

$$\hat{P}^-(k) = F(s(k))P(k-1)F^T(s(k-1)) + Q(k-1) \quad (16)$$

$$\begin{aligned}
K(k) &= \hat{P}^-(k)H^T[HP^-(k)H^T + R(k)] \quad (17) \\
\hat{s}(k) &= \hat{s}^-(k) + K(k)[Y(k) - H\hat{s}^-(k)] \\
P(k) &= [I - (K(k)H)]\hat{P}^-(k)
\end{aligned}$$

In equation 15, $\hat{s}^-(k)$ provides the apriori estimate of s . \hat{P}^- provides the associated covariance matrix where $Q(k-1)$ provides the covariance for the process noise $\omega(k-1)$. In equation 17, $K(k)$ is the Kalman gain, $R(k)$ being the covariance of observation noise $\eta(k)$. $\hat{s}(k)$ provides the estimated state vector s at k .

$$\hat{s}(0) = E[s(0)] \quad (18)$$

$$P(0) = E[(s(0) - E[s(0)])(s(0) - E[s(0)])^T] \quad (19)$$

In Figure 6, the path computation starts at n_a . Let the values of j and l are equal which is 2. At start, k is 1. Now s cannot be formed as minimum 2 previous travel costs are needed. Exploration proceeds with average travel cost for the edges. When n_c needs to be explored, value of k becomes 2 as one travel cost has been known connecting n_c to its predecessor n_a . s can be now formed as $X(1)$ is known. Again, n_a is the source and so $X(0)$ is 0. ξ is assumed to be $N(0.1, 0.1)$. At $k=2$, $s(1)$ takes the form $(1, \xi(0), \xi(1), X(0), X(1))^T$. Equation 15 and 17 are used to estimate $s(2)$ separately for all edges arising out of n_c to obtain X for each edge. From equations 18 and 19, $s(0)$ and $P(0)$ can be obtained. Let at n_g , $k=4$. Hence, $X(3)$ will be travel cost from n_e (predecessor of n_g) to n_g , $X(2)$ will be travel cost from n_c (predecessor of n_e) to n_e , $X(1)$ will be travel cost from n_a (predecessor of n_c) to n_c . Thus, $s(3) = (1, \xi(2), \xi(3), X(2), X(3))^T$ and $s(4) = (1, \xi(3), \xi(4), X(3), X(4))^T$ needs to be computed. This approach is different from Algorithm 1 in the way the X is estimated.

B. Results

The process of path computation is exactly similar to previous experiment. Only difference is in the estimation procedure of X , which is based on the bilinear state space model. The b and c are chosen as normal distribution. Along with the repetitions of path computations, the value ϕ , mean and covariance of b and c are increased from -0.4 to 0.4 and from -0.2 to 0.2 respectively. Negative values of ϕ produced too high estimates while values greater than 0.2 produced negative estimates. Similarly, mean and covariance values less than 0.1 produce high estimates and more than 0.1 produce negative estimates. Thus, 0.2 is found as the suitable value of ϕ and $N(0.1, 0.1)$ suits for both b and c . Also, the *regression_no* from 2 to 9 for each of 20, 40, 60 and 80 repetitive computation and average total path costs obtained on each case are plotted in Figure 7. The vertical bars marked from *Reg₂* to *Reg₉* represent the average total path costs for dynamic estimates based routes, which shows that they are 15% less on average than heuristic euclidean cost for all three maps in each set of repetitions. This difference is increased with the increase of *regression_no*, though the rate of increase is low, as the change of X itself is not broadly spread with standard deviation of 0.219 on average. The average total path cost increases with increase in number of repetitions as edge

travel cost increases with elapse of time. The observation $Y(k)$ developed during run-time is considered as signal and the values of ω are modified to increased the Signal-to-Noise Ratio (SNR) from 10dB to 50 dB along with the repetitions of path planning. The vertical bars marked 10dB, 25dB and 50dB in Figure 7 plots the average path costs obtained by changing the SNR for each *regression_no*. which shows that with the increase of SNR, the average travel cost decreases.

C. Path comparison

Part (a) of Figure 8 plots 3 single paths PathA, PathB and PathC obtained from Dijkstra's algorithm based on heuristic costs, statically estimated and dynamically estimated edge travel costs respectively for the same pair of source and destination nodes in Map 2 including only the variation induced by discharge of batteries. Here, P_{cA} , P_{cB} and P_{cC} stands for the general P_c vector explained in Section III for PathA, PathB and PathC respectively. P_{cA} , P_{cB} and P_{cC} have many common elements, despite having different elements. Thus, the total travel cost in these 3 paths are different. After obtaining the total travel costs of PathA, PathB and PathC, it can be stated that,

$$\sum P_{cB} < \sum P_{cA} \text{ by } 5\% \text{ and } \sum P_{cC} < \sum P_{cA} \text{ by } 15\%$$

This also establishes the proposal that heuristics based path planning can underestimate real edge travelling costs and lead to expensive paths. PathA and PathC in (b) and (c) of Figure 8 are obtained in Map 1 by heuristic based edge weights and dynamically estimated edge travel costs respectively, when floor condition is changed in dotted line zone to moderately rough and solid line zone to lightly rough after 20 calls for route computation. PathA in both (b) and (c) contains edges in both rough zones in the floor, while PathC in (b) clearly avoids the zone with moderate roughness, though having few edges in the lightly rough zone. This happens because Dijkstra's algorithm finds that cost incurred in traversing the lightly rough zone to be less than that of the additional edges required to avoid the zone. This proves that modification of Dijkstra's algorithm using dynamically estimated travel cost does not disrupt the computational robustness of the algorithm. Also, when the lightly rough zone is made heavily rough, PathC deviates to other direction and adding more nodes. Thus again, estimated travel times of edges help Dijkstra's algorithm to find a cost effective path.

D. Real cost saving for paths

In (b) of Figure 8, there are total 12 edges from the 2 rough zones comprised in PathA. The path cost of PathA obtained using heuristic weights is not the correct one as travel costs of each of these 12 edges are more than assumed. Let, a variable δ accounts for the additional edge costs in each edge. Path cost of PathA is obtained as 98.210 from results, but in reality path cost of PathA should be $(98.210 + 12*\delta)$. The value of δ can never be zero as changes in environment and batteries will always be present. When more zones will have changed floor conditions, more edges will have increased edge cost. So, the coefficient of δ will increase and also the true value

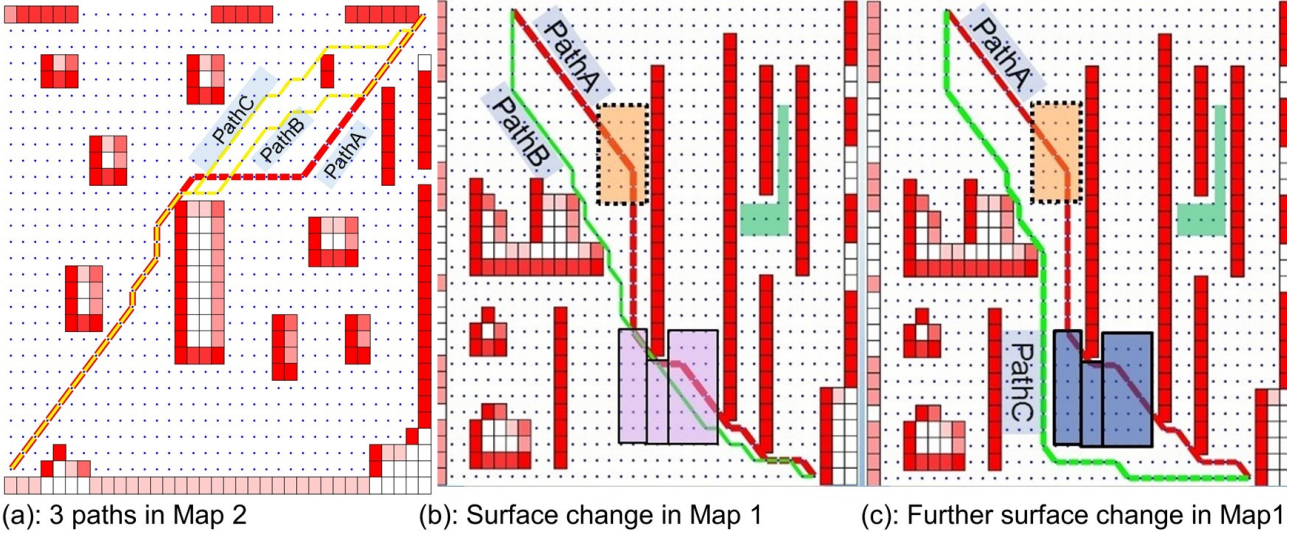


Fig. 8: Paths in different conditions

of travel cost of paths. Thus, the difference between travel costs of paths obtained by heuristic cost and estimated travel time will always increase with the increase of hostility in the environment.

VII. DISCUSSION AND CONCLUSION

The travel times of edges are identified as one of the cost coefficients in internal automated logistics. A formulation is devised to estimate travel times online during path computation considering its time-varying components. Moreover, suitable observations for travel time are recorded in scenarios with analogy to real factory in a scaled platform developed in the laboratory. They are instrumental for feeding into estimation algorithms to estimate travel time. Path is found using Dijkstra's algorithm based on both heuristic weights of edges and estimated edge travel times as weights. Results show that paths computed using travel time as weights of edges have lesser total path cost than that of obtained by heuristic weights. Environmental factors based costs are modeled as Gaussian process regression from already obtained finite measured data in [21], but it does not include time-varying changes in batteries and environment. On the other hand, sampling based heuristic path planning [7], [15] requires to explore a significant portion of the graph needs to find a suitable path, which is computationally expensive. Nevertheless, in this work, the cost of traversing every edge is estimated, which facilitates to apply deterministic path planning algorithms like Dijkstra's algorithm, Bellmont-Ford algorithm *et cetera*. The approach used in single robot case in this work can be extended in multi-task scenarios using travel time as cost parameter in all the MRs in the system. During the run-time of MRS, every estimated value of travel time has context depending on various environmental and inherent factors. Travel time of one AGV can provide contextual to others and contribute in estimating travel cost for them. This enhances further investigation towards implementing collaborative or collective intelligence in MRS.

REFERENCES

- [1] Markus W Achtelik, Steven Weiss, Maria Chli, and Roland Siegwart. Path planning for motion dependent state estimation on micro aerial vehicles. In *Robotics and Automation (ICRA), 2013 IEEE International Conference on*, pages 3926–3932. IEEE, 2013.
- [2] Maram Alajlan, Anis Koubaa, Imen Chaari, Hachemi Bennaceur, and Adel Ammar. Global path planning for mobile robots in large-scale grid environments using genetic algorithms. In *Individual and Collective Behaviors in Robotics (ICBR), 2013 International Conference on*, pages 1–8. IEEE, 2013.
- [3] Haluk Bayram and H Işıl Bozma. Coalition formation games for dynamic multirobot tasks. *The International Journal of Robotics Research*, 35(5):514–527, 2016.
- [4] Patric Beinschob and Christoph Reinke. Graph slam based mapping for agv localization in large-scale warehouses. In *Intelligent Computer Communication and Processing (ICCP), 2015 IEEE International Conference on*, pages 245–248. IEEE, 2015.
- [5] Subhrajit Bhattacharya, Maxim Likhachev, and Vijay Kumar. Multi-agent path planning with multiple tasks and distance constraints. In *Robotics and Automation (ICRA), 2010 IEEE International Conference on*, pages 953–959. IEEE, 2010.
- [6] Xiong Chen, Yingying Kong, Xiang Fang, and Qidi Wu. A fast two-stage aco algorithm for robotic path planning. *Neural Computing and Applications*, 22(2):313–319, 2013.
- [7] Marcello Cirillo, Tansel Uras, and Sven Koenig. A lattice-based approach to multi-robot motion planning for non-holonomic vehicles. In *Intelligent Robots and Systems (IROS 2014), 2014 IEEE/RSJ International Conference on*, pages 232–239. IEEE, 2014.
- [8] Mitchell Colby, Jen Jen Chung, and Kagan Tumer. Implicit adaptive multi-robot coordination in dynamic environments. In *Intelligent Robots and Systems (IROS), 2015 IEEE/RSJ International Conference on*, pages 5168–5173. IEEE, 2015.
- [9] S Hamid Dezfoulian, Dan Wu, and Imran Shafiq Ahmad. A generalized neural network approach to mobile robot navigation and obstacle avoidance. In *Intelligent Autonomous Systems 12*, pages 25–42. Springer, 2013.
- [10] M. B. Dias, R. Zlot, N. Kalra, and A. Stentz. Market-based multi-robot coordination: A survey and analysis. *Proceedings of the IEEE*, 94(7):1257–1270, July 2006.
- [11] Mohamed Elbanhawi and Milan Simic. Sampling-based robot motion planning: A review. *IEEE Access*, 2:56–77, 2014.
- [12] Alessandro Farinelli, Luca Iocchi, and Daniele Nardi. Distributed on-line dynamic task assignment for multi-robot patrolling. *Autonomous Robots*, pages 1–25, 2016.
- [13] B Gerkey and Maja J Mataric. Are (explicit) multi-robot coordination and multi-agent coordination really so different. In *Proceedings of the AAAI spring symposium on bridging the multi-agent and multi-robotic research gap*, pages 1–3, 2004.

- [14] Thi Thoa Mac, Cosmin Copot, Duc Trung Tran, and Robin De Keyser. Heuristic approaches in robot path planning: A survey. *Robotics and Autonomous Systems*, 86:13–28, 2016.
- [15] Neil Mathew, Stephen L Smith, and Steven L Waslander. Optimal path planning in cooperative heterogeneous multi-robot delivery systems. In *Algorithmic Foundations of Robotics XI*, pages 407–423. Springer, 2015.
- [16] R. Parasuraman, K. Kershaw, P. Pagala, and M. Ferre. Model based on-line energy prediction system for semi-autonomous mobile robots. In *2014 5th International Conference on Intelligent Systems, Modelling and Simulation*, pages 411–416, 2014.
- [17] MB Priestley. Current developments in time series modelling. *Journal of Econometrics*, 37(1):67–86, 1988.
- [18] Lluís Ribas-Xirgo and Ismael F Chaile. An agent-based model of autonomous automated-guided vehicles for internal transportation in automated laboratories. In *ICAART (I)*, pages 262–268, 2013.
- [19] Lluís Ribas-Xirgo, Joaquín Saiz-Alcaine, Jonatan Trullàs-Ledesma, and A Josep Velasco-González. An approach to a formalized design flow for embedded control systems of micro-robots. In *Industrial Electronics, 2009. IECON'09. 35th Annual Conference of IEEE*, pages 2187–2192. IEEE, 2009.
- [20] Indranil Saha, Rattanachai Ramaithitima, Vijay Kumar, George J Pappas, and Sanjit A Seshia. Implan: scalable incremental motion planning for multi-robot systems. In *Cyber-Physical Systems (ICCPs), 2016 ACM/IEEE 7th International Conference on*, pages 1–10. IEEE, 2016.
- [21] Junghun Suh and Songhwai Oh. A cost-aware path planning algorithm for mobile robots. In *Intelligent Robots and Systems (IROS), 2012 IEEE/RSJ International Conference on*, pages 4724–4729. IEEE, 2012.
- [22] Yong Zhang, Dun-wei Gong, and Jian-hua Zhang. Robot path planning in uncertain environment using multi-objective particle swarm optimization. *Neurocomputing*, 103:172–185, 2013.